

Article

Production and Potential Genetic Pathways of Three Different Siderophore Types in *Streptomyces tricolor* Strain HM10

Medhat Rehan ^{1,2,*}, Hassan Barakat ^{3,4,*}, Ibtesam S. Almami ⁵, Kamal A. Qureshi ^{6,7}
and Abdullah S. Alsohim ¹

- ¹ Department of Plant Production and Protection, College of Agriculture and Veterinary Medicine, Qassim University, Buraydah 51452, Saudi Arabia; a.alsohim@qu.edu.sa
² Department of Genetics, Faculty of Agriculture, Kafrelsheikh University, Kafr El-Sheikh 33516, Egypt
³ Department of Food Science and Human Nutrition, College of Agriculture and Veterinary Medicine, Qassim University, Buraydah 51452, Saudi Arabia
⁴ Food Technology Department, Faculty of Agriculture, Benha University, Moshthor 13736, Egypt
⁵ Department of Biology, College of Science, Qassim University, Buraydah 52571, Saudi Arabia; I.almami@qu.edu.sa
⁶ Department of Pharmaceutics, Unaizah College of Pharmacy, Qassim University, Unaizah 51911, Saudi Arabia; ka.qurisha@qu.edu.sa
⁷ Faculty of Biosciences and Biotechnology, Invertis University, Bareilly 243123, Uttar Pradesh, India
* Correspondence: m.rehan@qu.edu.sa (M.R.); haa.mohamed@qu.edu.sa (H.B.)

Abstract: Siderophores are iron-chelating low-molecular-weight compounds that bind iron (Fe³⁺) with a high affinity for transport into the cell. The newly isolated strain *Streptomyces tricolor* HM10 secretes a pattern of secondary metabolites. Siderophore molecules are the representatives of such secondary metabolites. *S. tricolor* HM10 produces catechol, hydroxamate, and carboxylate types of siderophores. Under 20 μM FeCl₃ conditions, *S. tricolor* HM10 produced up to 6.00 μg/mL of catechol siderophore equivalent of 2,3-DHBA (2,3-dihydroxybenzoic acid) after 4 days from incubation. In silico analysis of the *S. tricolor* HM10 genome revealed three proposed pathways for siderophore biosynthesis. The first pathway, consisting of five genes, predicted the production of catechol-type siderophore similar to petrobactin from *Bacillus anthracis* str. Ames. The second proposed pathway, consisting of eight genes, is expected to produce a hydroxamate-type siderophore similar to desferrioxamine B/E from *Streptomyces* sp. ID38640, *S. griseus* NBRC 13350, and/or *S. coelicolor* A3(2). The third pathway exhibited a pattern identical to the carboxylate xanthoferrin siderophore from *Xanthomonas oryzae*. Thus, *Streptomyces* strain HM10 could produce three different types of siderophore, which could be an incentive to use it as a new source for siderophore production in plant growth-promoting, environmental bioremediation, and drug delivery strategy.

Keywords: siderophore; catechol-type; hydroxamate-type; carboxylate-type; *S. tricolor* HM10



Citation: Rehan, M.; Barakat, H.; Almami, I.S.; Qureshi, K.A.; Alsohim, A.S. Production and Potential Genetic Pathways of Three Different Siderophore Types in *Streptomyces tricolor* Strain HM10. *Fermentation* **2022**, *8*, 346. <https://doi.org/10.3390/fermentation8080346>

Academic Editors:
Alessandro Robertiello and
Francesca Berini

Received: 18 May 2022

Accepted: 20 July 2022

Published: 22 July 2022

Publisher's Note: MDPI stays neutral with regard to jurisdictional claims in published maps and institutional affiliations.



Copyright: © 2022 by the authors. Licensee MDPI, Basel, Switzerland. This article is an open access article distributed under the terms and conditions of the Creative Commons Attribution (CC BY) license (<https://creativecommons.org/licenses/by/4.0/>).

1. Introduction

On the planet Earth, the atmosphere is very rich in oxygen. Under exposure to this oxygen-rich state, the free ferrous iron (Fe²⁺) oxidizes to the insoluble ferric iron (Fe³⁺), reducing the bioavailability of ferric iron. Microorganisms growing in an aerobic environment require iron for many cellular enzymes as cofactors. These primary and secondary metabolic enzymes provide various cellular functions such as DNA replication, reduction of oxygen to generate PMF (proton motive force), and subsequent synthesis of ATP, protecting the cell from oxidative stress and other essential purposes [1–4]. In an iron-deficient environment, microorganisms acquire iron by producing iron-chelating low-molecular-weight (between 500 and 2000 daltons) compounds called siderophores. Siderophores chelate iron (Fe³⁺) with high affinity and form a ferric–siderophore complex outside the cell that is imported into the bacterial cytosol through transporters in the extracellular membrane [1,2,4].

Siderophores are generally categorized based on the functional group involved in iron chelating. This active group could be catecholate, hydroxycarboxylate, or hydroxamate [5,6]. Catechol-type chelates Fe^{3+} via hydroxyl groups of catechol rings, and the compound 2,3-dihydroxybenzoic acid (DHBA) is considered its precursor (i.e., petrobactin from *Bacillus anthracis*, enterobactin from *E. coli*, and *Pseudomonas aeruginosa*) [7,8]. Hydroxamate-type siderophores bind with iron through a carboxyl group that is attached to adjacent nitrogen atoms of thiazoline and oxazoline rings (i.e., desferrioxamine B/E from *Streptomyces griseus* and/or *S. coelicolor* A3(2) and ferrichrome from *Ustilago sphaerogena*) [5,9,10]. In the hydroxycarboxylate type, siderophores utilize the N-hydroxyl group with an oxygen atom to bind with Fe^{3+} (i.e., staphyloferrin A and B from *Staphylococci*) [11]. The fourth group with combinations from the above types has also been identified and named “mixed type” [12].

In bacteria, two main pathways for siderophore biosynthesis have been identified [1,13–15]. The first pathway utilizes both multienzymes, nonribosomal peptide synthetase (NRPS), and polyketide synthases (PKSs) and is identified in *Streptomyces scabies* 87.22 [4]. The second pathway uses NRPS-independent siderophore (NIS) synthetases. Furthermore, the ferric–siderophore complex requires outer membrane receptor protein (i.e., the ferrichrome transporter, FepA) [16]. A periplasmic-binding protein shuttles the Fe^{3+} –siderophore complex to the ABC-type transporter in the cell’s inner membrane through ATP hydrolysis [17].

Siderophores have wide applications and are utilized in multiple fields, including agriculture, pharmacy, medicine, and environmental applications [18–24]. In agriculture and the environment, siderophores increase the growth and yield of various plants, woods, and textiles through the improvement in iron acquisition [24–26]. Moreover, hydroxamate-type siderophore plays an important role in immobilizing the metals in soil [22,27]. In biocontrol, siderophores are considered a growth inhibitor for various phytopathogenic fungi and toxic algal blooms [22,28]. In the medicinal applications and iron-overload diseases (hemosiderosis, β -thalassemia, hemochromatosis, and accidental iron poisoning), there is a requirement to remove iron from the body that can be treated with siderophore-based drugs. The hydroxamate-based siderophore (desferrioxamine B), which is isolated from *Streptomyces pilosus*, was used for the first time in the treatment of iron overload (1960) [21,29]. The iron-conveying ability of siderophore is used to deliver drugs. The drug delivery occurred in cells by forming conjugates among antimicrobials such as albomycins and siderophores [20,22,30,31]. Siderophores have potential use as iron chelators in treating cancers, e.g., dexrazoxane, desferrioxchelins, desferriothiocin, and O-trenox [32,33].

Furthermore, siderophores can be utilized to rescue non-transferrin-bound iron in the blood serum. Since siderophores produced by *Klebsiella pneumoniae* can act as an antimalarial agent, siderophores have been used to treat malaria caused by *Plasmodium falciparum* [33,34]. The bacteria, *Streptomyces*, produce a wide variety of siderophore types (i.e., hydroxamate-type siderophores [35–38], catechol-type siderophores [39,40], hydroxycarboxylate-type siderophores [41]). The present work aimed to (i) characterize the siderophore production in *S. tricolor* HM10 isolated from Qassim, Saudi Arabia; (ii) determine the siderophore types produced by the mentioned strain; (iii) identify the proposed pathways involved in each type of production; and (iv) identify the probability of using strain HM10 as a new source for siderophore production.

2. Materials and Methods

2.1. Media and Growth Condition

Streptomyces tricolor HM10 (Accession: MN527236) [42] was selected for the current study. For regular growth and maintenance, Tryptic Soy Agar/broth (TSA/B) medium (ingredients (g/l), peptic digest of soybean meal, 5.0; sodium chloride, 5.0; agar, 15.0; pH 7.5) was used for hyphae production. Glucose soyabean meal agar (GSA) (soybean meal, 10.0; glucose, 10.0; CaCO_3 , 1.0; NaCl, 10.0; agar, 15 (g/l) and pH adjusted to 7.0) was applied for sporulation. King’s medium B base comprising (g/l) peptone, 20.0; K_2HPO_4 , 1.50; MgSO_4 , 7.0; H_2O , 1.50; agar, 15.0; pH 7.2) was used for siderophore detection and production at 28 °C.

2.2. Detection of Siderophore Production

The universal chemical assay (Chrome Azurol S, CAS assay) was applied to detect siderophore production in *S. tricolor* HM10 [43]. CAS was prepared by dissolving 60.5 mg from chrome azurol S in 50 mL ddH₂O, and 72.9 mg from hexadecyltrimethyl ammonium bromide (HDTMA) was dissolved in 40 mL ddH₂O and added to 10 mL Fe³⁺ solution (162 mg from FeCl₃ in 83.3 µL/HCL in 100 mL ddH₂O). The mixed solution (coming from the addition of HDTMA slowly to CAS with the formation of a dark blue color) was then autoclaved. The autoclaved King's medium and CAS indicator solution were mixed together after cooling to 50 °C with a 9:1 ratio and poured into sterile Petri dishes. In the liquid medium, siderophore detection was achieved in response to iron concentrations (0, 0.5, and 20 µM).

2.3. Catechol-Type Siderophore

To detect the catechol-type siderophore, Arnow's assay was performed. Briefly, 1 mL culture supernatant/uninoculated medium, 1 mL HCl (0.5 M), 1 mL nitrite-molybdate reagent (NaNO₂, 10 g and Na₂MoO₄, 10 g dissolved in 100 mL ddH₂O), and 1 mL NaOH (1 M) were mixed. Catechol siderophore's presence is indicated by pink color formation, whereas the control remains colorless [44]. Absorbance was measured at 500 nm (EPOCH2TS, BioTek, Winooski, VT, USA).

2.4. Hydroxamate-Type Siderophore

The culture supernatant was subjected to Atkin's assay for hydroxamate-type siderophores detection. The assay was performed by combining the following components: 0.5 mL from culture/uninoculated medium and 2.5 mL from Atkin's reagent (0.1771 g Fe(ClO₄)₃ in 100 mL ddH₂O containing 1.43 mL HClO₄ [45]). The reaction was incubated at room temperature for 5 min for full color development. Absorbance at 480 nm was recorded with an EPOCH2TS plate reader (BioTek, Winooski, VT, USA).

2.5. Carboxylate-Type Siderophore

The presence of carboxylate siderophore was detected by spectrophotometric assay with minor modification [46]. Briefly, 50 µL from culture supernatant/uninoculated medium, 50 µL from CuSO₄ (250 µM), and 100 µL from acetate buffer (pH 4) were mixed. The absorption peak was monitored in the 200–280-nm wavelength range.

2.6. Growth Pattern and Siderophore Production

In response to iron concentrations, growth was performed for the optimal condition to maximize the catechol-, hydroxamate-, and carboxylate-type siderophore production. A fresh seed culture of *S. tricolor* HM10 was inoculated onto King's medium at 28 °C for 4 days on a rotary shaker at 170 rpm. Samples for siderophore quantification were taken at different incubation times (days, 0, 1, 2, 3, and 4) in response to different concentrations of FeCl₃ (0, 0.5, 1, 5, and 20 µM). Samples were centrifuged at 10,000 rpm for 5 min, and culture filtrates were used to detect siderophore production by Arnow's and Atkin's assays. A standard curve was generated by a known concentration of 2,3-dihydroxybenzoic acid (2,3-DHBA).

2.7. Whole-Genome Sequencing

DNA was extracted from *S. tricolor* HM10 via the CTAB method [47]. The purity of isolated DNA was tested by a NanoDrop spectrophotometer (1000) and Qubit™ assay (Life Technologies, Carlsbad, CA, USA). The whole genome was sequenced by Oxford Nanopore technology (Department of Molecular, Cellular, and Biomedical sciences, University of New Hampshire, Durham, NH, USA), assembled (using the EPI2ME Labs platform employing Flye version FLYE 2.8.1-b1676 [48] or assembly, Racon version v1.4.16 for a first-step polishing, followed by a second polishing step using Medaka version 1.5.0) and annotated by NCBI, and given the accession number JAJREA000000000 (<https://www.ncbi.nlm.nih>).

[gov/nucleotide/JAJREA000000000](https://www.ncbi.nlm.nih.gov/nucleotide/JAJREA000000000) (accessed on 16 December 2021) [49]. The statistics of the sequenced genome are presented in Table S1.

2.8. Genome Sequence Analysis of Siderophore Pathways

An in silico analysis of the genome was performed to identify siderophore production pathways and other secondary metabolites and natural compounds. We used blast search at NCBI (<https://www.ncbi.nlm.nih.gov/> (accessed on 20 April 2022)), antiSMASH online software [50], Pfam: the protein families database [51], and the Minimum Information about a Biosynthetic Gene cluster (MIBiG) [52].

2.9. Phylogenetic Tree Construction

For molecular phylogenetic tree construction, the amino acid sequences of IucA/IucC family protein from the *S. tricolor* strain HM10 were aligned with homologous protein sequences recovered from the GenBank database and other similar proteins published in the literature via ClustalW in MEGA11 software [53]. The following parameters were applied in tree construction: Maximum likelihood as a statistical method, Jones–Taylor–Thornton (JTT) model, and nearest-neighbor-interchange (NNI) as an ML heuristic method with 1000 bootstrap replicates [53].

2.10. Statistical Analysis

All data in siderophore production were presented as mean \pm standard deviation of the mean using the Student's t-test. The statistical significance of the differences between treatments was determined using two-way ANOVA and Tukey's post hoc test ($p < 0.0001$) in STATISTICA for Windows (StatSoft 2005) [54]. To measure the significant differences between four days of incubation and iron concentrations, the LSD values were calculated to obtain direct comparisons among treatments' means.

3. Results

3.1. Siderophore Detection in Solid and Liquid Medium

For the initial detection of siderophore production, *S. tricolor* HM10 was grown on King's B agar medium supplemented with CAS under low-iron conditions (without the addition of any external iron) for 48 h at 28 °C. A color change around the bacterial inoculum with an orange halo pointed to siderophore production (Figure 1I). In fermented broth, supernatants were collected from cultures growing for 48 h with 0, 0.5, and 20 μ M from FeCl₃ by centrifugation, and 120 μ L was added to the wells in the prepared CAS plates. A color change was observed in the form of an orange halo around the wells, approximately 22 mm in diameter. In contrast, no color change was exhibited around the well containing the uninoculated medium (Figure 1II).

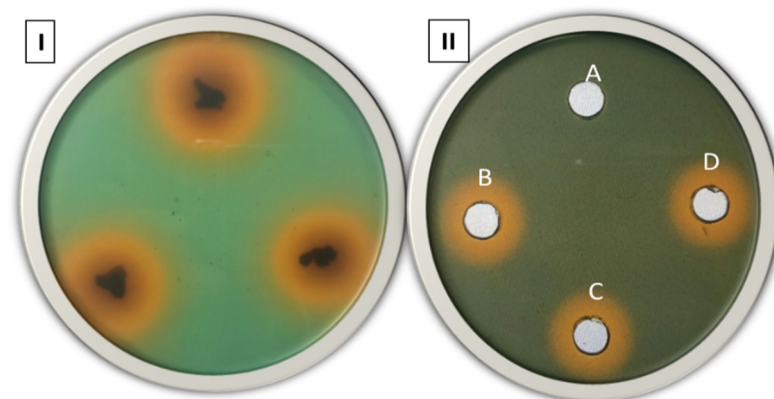


Figure 1. Siderophore production by *S. tricolor* HM10 on King's B solid medium (I) and liquid medium (II) was detected by the orange halo around wells. (A) Media control, (B) 0 μ M FeCl₃, (C) 0.5 μ M FeCl₃, and (D) 20 μ M FeCl₃.

3.2. Chemical and Production Characterization of Siderophore

To detect the chemical type of siderophore produced by the *S. tricolor* strain HM10, Arnow's and Atkin's assays were applied for the catechol and hydroxamate types of siderophore, respectively. The supernatant of the culture broth grown for 48 h with no added iron was subjected to both assays against the uninoculated medium control. A pink/red color developed in the case of Arnow's assay with the culture broth supernatant, indicating catechol-type siderophore production (Figure 2A(I,II)). In contrast, a wine (faint) color was observed in the Atkin's assay, pointing to the production of hydroxamate-type siderophore in comparison with the uninoculated medium (Figure 2A(III,IV)). In the Arnow analysis, a standard curve for siderophore production was generated during the growth curve with a known concentration of 2,3-DHBA. Samples were collected from cultures grown for four days with different iron concentrations. The tested samples indicated that the highest catechol-type siderophore production was achieved after 4 days at 5.45 and 6.00 $\mu\text{g/mL}$ equivalent of 2,3-DHBA at 5 and 20 μM iron, respectively. In contrast, the production under 0, 0.5, and 1 μM iron stayed almost constant during the entire growth period (Figure 2B). The production of hydroxamate siderophore continued to increase with an elongated incubation time, and the highest production was measured on day 4 under 5 and 20 μM iron (Figure 2C). Carboxylate siderophore production increased gradually under 0.5 and 1 μM FeCl_3 and reached a peak on day 4 while the production under 5 and 20 μM iron increased in the beginning (days 1 and 2) and dropped off on day 4 (Figure 2D). Based on the statistical significance of the differences between treatments, two-way ANOVA determined that no significant differences were detected along with incubation time.

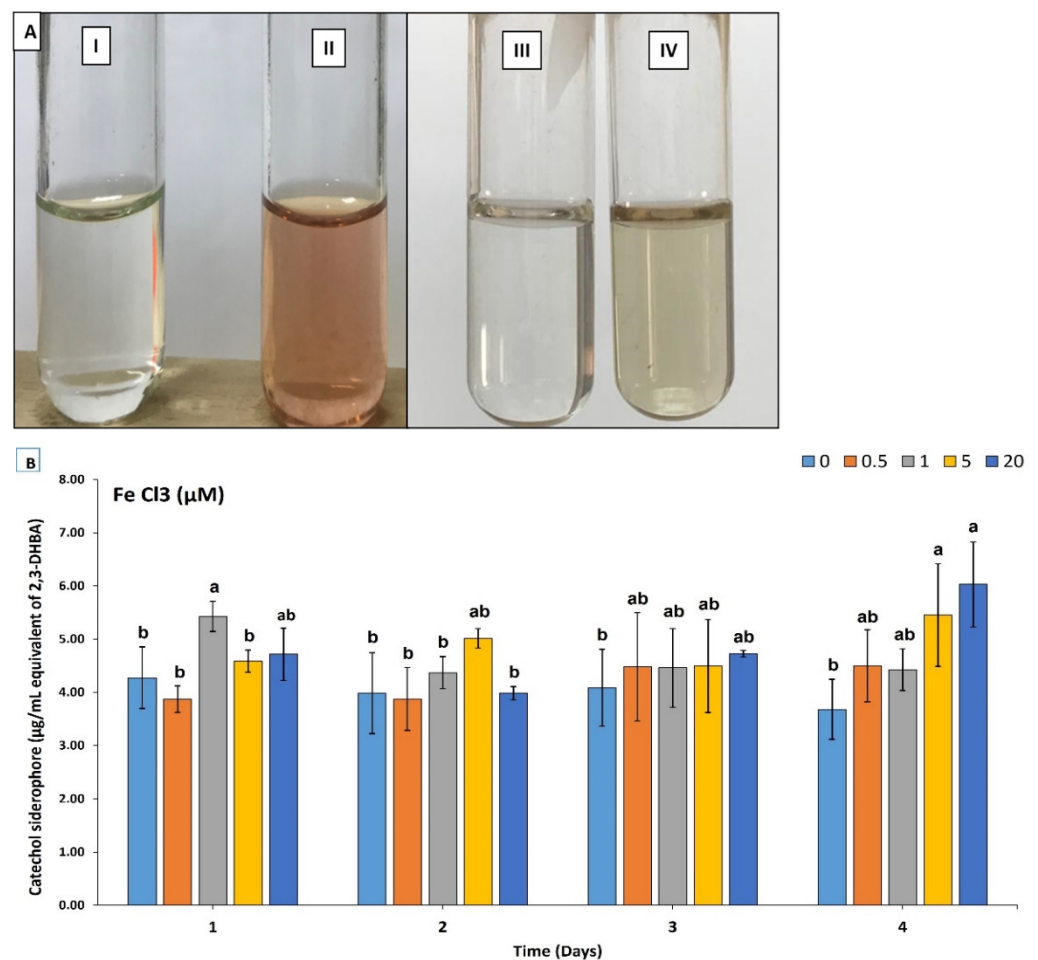


Figure 2. Cont.

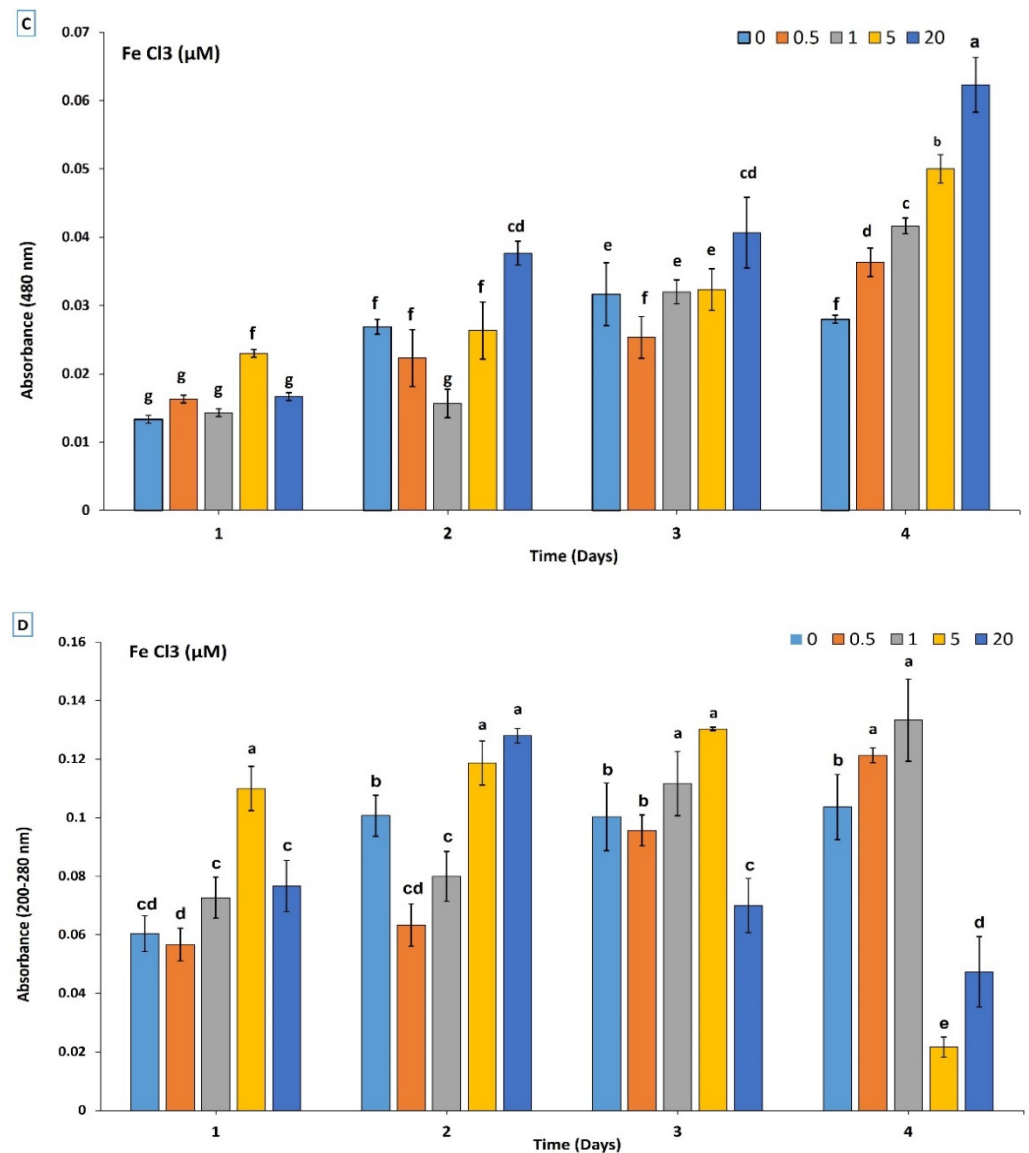


Figure 2. (A) Arnow’s and Atkin’s assays for catechol- and hydroximate-type siderophore detection. (I and III) indicate no color detection with the uninoculated culture; (II) shows a catechol-type siderophore with a positive color (pink color). In contrast, (IV) indicates hydroximate-type siderophores in culture inoculated with *S. tricolor* HM10 for 48 h. (B–D) Time course production of siderophores in response to iron. (B) Production of catechol-type siderophore, (C) production of hydroximate-type siderophore, and (D) production of carboxylate-type siderophore. Results are produced from three replicates ($n = 3$), ^{a,b,c,d,e,f,g}; Bars not sharing similar letters are significantly different ($p > 0.05$).

3.3. Genome Analysis for Siderophores Pathways

In silico analysis of the *S. tricolor* HM10 genome revealed three different possible pathways for siderophore production. One pathway predicted catechol siderophore biosynthesis, the second pathway predicted hydroximate siderophore production, and the third pathway predicted carboxylate siderophore biosynthesis.

3.3.1. Catechol-Type Siderophore Pathway

The proposed catechol pathway is closely related to the petrobactin siderophore pathway found in *Bacillus anthracis* str. Ames when compared at MIBiG (Figure 3A). This pathway contains 5 genes 4717 bp in length on contig 28.1 with up to 85% similarity to those

found in *Streptomyces* sp. BK340 by ClusterBlast (Figure S1). The first gene is predicted to encode an acetyltransferase (LT493_17645), which is hypothesized to acetylate hydroxyornithine to produce acetylated-hydroxyornithine or hydromevalonyl-hydroxyornithine, and the second gene produces a ferric iron reductase FhuF-like transporter (LT493_17650) that liberates iron from the Fe³⁺-siderophore complex through the reduction process. The third gene is predicted to encode the siderophore biosynthetic protein (IucA/IucC family protein, LT493_17655), which consists of three domains: (i) a peptidyl carrier protein (thiolation), (ii) an adenylation, and (iii) condensation domains. This enzyme is responsible for the assembly of a wide array of amino, carboxy, and hydroxy acids in variable combinations to produce variety polypeptides. Moreover, the fourth gene encodes an iron transport protein (LT493_17660). The fifth gene product is predicted to be a diamino butyrate-2-oxoglutarate transaminase family protein with transaminase activity (LT493_17665), which is proposed to convert aspartate to 2,4-diamino butyrate, transferring the amino group from glutamate (Figure 3B).

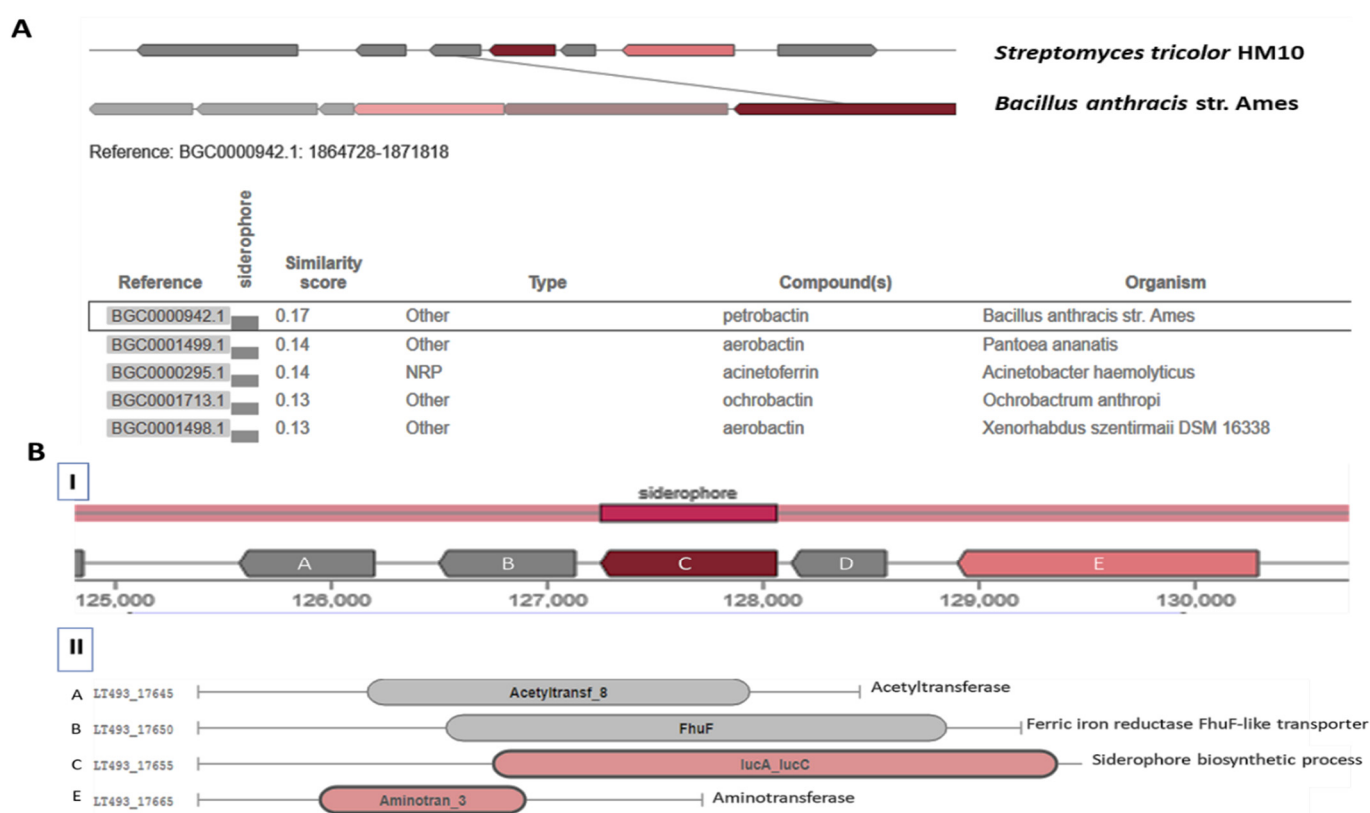


Figure 3. (A) The comparison between the proposed catechol-type siderophore gene cluster (dark red gene) in *S. tricolor* HM10 and the identified catechol-type siderophore pathway in *Bacillus anthracis* str. Ames with a similarity score of 0.17 on the MIBiG website. (B) The proposed gene cluster for the catechol-type siderophore in *S. tricolor* HM10 was identified based on the Pfam website. (I) The siderophore pathway located in contig_28.1 from the genome sequence; (II) genes involved in siderophore production: A, acetyltransferase; B, Ferric iron reductase FhuF; C, IucA/IucC family protein; D, iron transporter; and E, aminotransferase.

3.3.2. Hydroxamate-Type Siderophore Pathway

In the continued analysis of the entire genome, a hydroxamate siderophore pathway was found in contig_10.2 with an 8775-bp DNA length. The proposed pathway contains eight genes predicted to produce siderophore closely related to desferrioxamine B/E found in *Streptomyces* sp. ID38640, *S. griseus* NBRC 13350, and/or *S. coelicolor* A3(2) (Figure 4A). The similarity between this pathway and those found in *S. coelicolor* A3(2) and *S. griseus* NBRC 13,350 reached 83% and 100%, respectively (Figure S2), when compared

with KnownClusterBlast at MIBiG. The entire pathway contains the following genes: (1) a siderophore-interacting protein (LT493_03445) with ferric reductase activity and proposed to catalyze the release of iron from iron–siderophore complex; (2) a lysine decarboxylase (LT493_03450, *desA*) that is hypothesized to decarboxylate L-lysine (lysine is a precursor for desferrioxamine siderophore biosynthesis) to 1,5-pentanediamine (cadaverine); (3) a lysine N(6)-hydroxylase/L-ornithine N(5)-oxygenase family protein (LT493_03455, *desB*) that *N*-hydroxylates cadaverine to produce *N*-hydroxycadaverine; (4) an acetyltransferase (LT493_03460, *desC*) that is proposed to *N*-acylate the *N*-hydroxycadaverine to produce *N*-hydroxy-*N*-succinylcadaverine or *N*-hydroxy-*N*-acetylcadaverine; (5) an *IucA*/*IucC* family protein (LT493_03465, *desD*) or ATP-dependent siderophore synthetase, which is proposed to produce desferrioxamine E/B siderophore (ferrioxamine B is derived from two units of *N*-succinyl-*N*-hydroxycadaverine and one of *N*-acetyl-*N*-hydroxycadaverine while three molecules of *N*-hydroxy-*N*-succinylcadaverine convert into desferrioxamine E); (6) a ferric iron reductase FhuF-like transporter (LT493_03470), which is suggested to be involved in iron release from the hydroxamate-type siderophore in the cytoplasm; and (7) a beta-*N*-acetylhexosaminidase (LT493_03475, *desF*) with hydrolase activity that is proposed to release iron from ferric-siderophore and (8) DUF4429 domain-containing protein (LT493_03480) with an unknown function (Figure 4B).

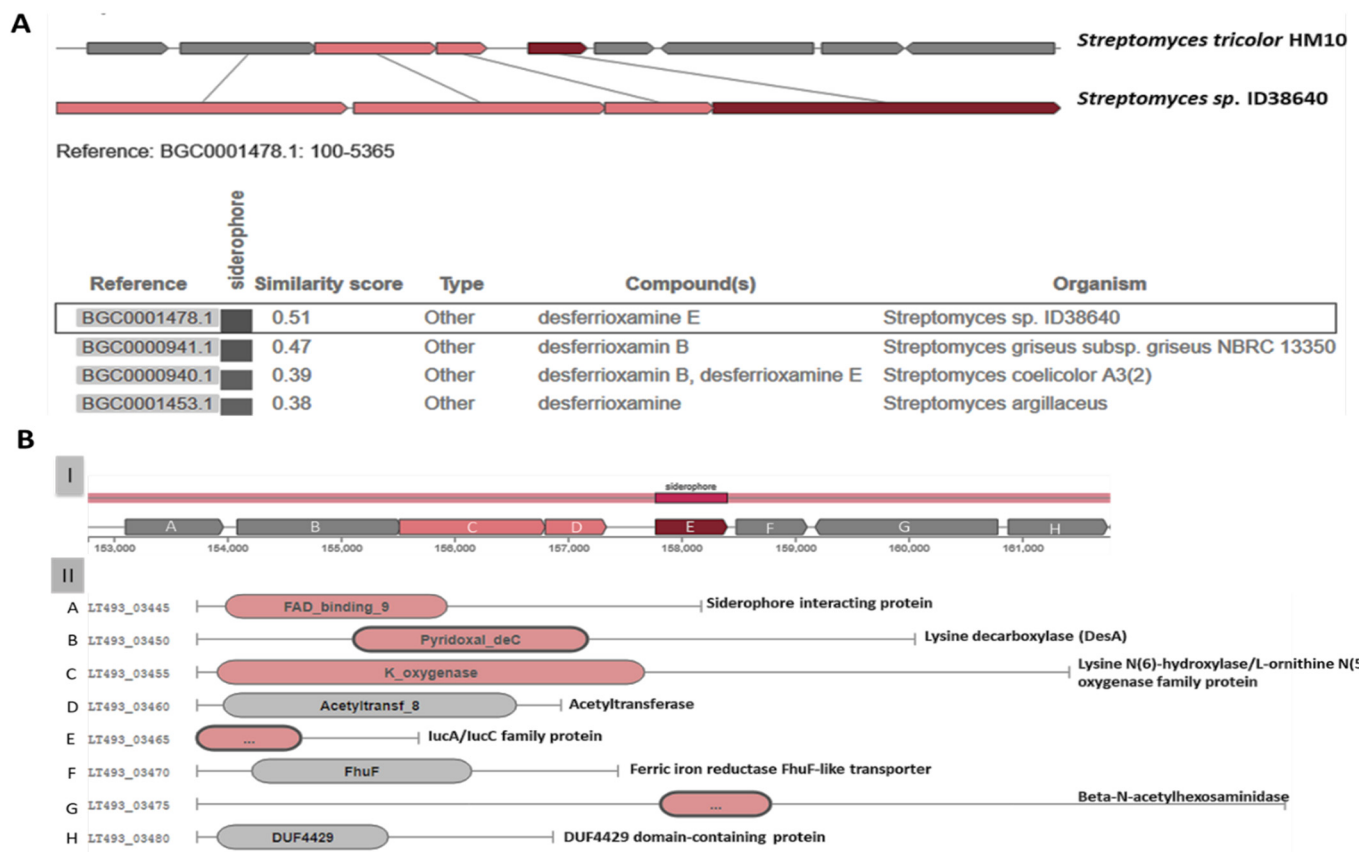


Figure 4. (A) The comparison between the proposed hydroxamate-type siderophore gene cluster (dark red and orange genes) in *S. tricolor* HM10 and the identified hydroxamate desferrioxamine B/E siderophore from *Streptomyces* sp. ID38640 and *S. griseus*, with similarity scores of 0.51 and 0.47, respectively, on the MIBiG website. (B) The proposed hydroxamate gene cluster in *S. tricolor* HM10 was identified based on the Pfam website. (I) Siderophore gene cluster in contig_10.2 from the genome sequence; (II) genes involved in siderophore biosynthesis: A, siderophore-interacting protein; B, lysine decarboxylase; C, lysine N(6)-hydroxylase/L-ornithine N(5)-oxygenase family protein; D, acetyltransferase; E, *IucA*/*IucC* family protein; F, ferric iron reductase FhuF-like transporter; G, beta-*N*-acetylhexosaminidase; and H, DUF4429 domain-containing protein.

3.3.3. Carboxylate-Type Siderophore Pathway

The third predicted pathway is involved in carboxylate siderophore biosynthesis. This pathway exists in contig_52.1 with nucleotides 11,052 bp in size. The proposed pathway showed similarity with the xanthoferrin siderophore found in *Xanthomonas oryzae* pv. *Oryzae* KACC 10331 (Figure 5A). In ClusterBlast, the most closely related pathway found in *S. griseoruber* DSM 40281 with similarity reached 81% (Figure S3). The proposed pathway contains seven genes that are predicted to encode the following: (1) a pyridoxal phosphate-dependent aminotransferase (LT493_32205) predicted to transfer an amino group to the siderophore precursor and produce amine substrate; (2) a transcriptional regulator (LT493_32210), which is hypothesized to control siderophore biosynthesis; (3) a VWA domain-containing protein (LT493_32220) with an unknown function; (4) an IucA/IucC family siderophore biosynthesis protein (LT493_32225) predicted to catalyze amide bond formation between an amine substrate and citric acid (monoamide or monoester derivatives) as a source for carboxylate siderophore; (5) IucA/IucC family siderophore biosynthesis protein and ferric iron reductase FhuF-like transporter (LT493_32230), hypothesized to condense different units (from the previous product or mix with other derivatives) based on the final siderophore product while FhuF will act in iron release from siderophore; (6) an Rdx family protein (family of selenoproteins) (LT493_32240) with oxidoreductase function possibility; and (7) nucleotidyltransferase family protein (LT493_32250) with an unknown function in siderophore biosynthesis (Figure 5B).

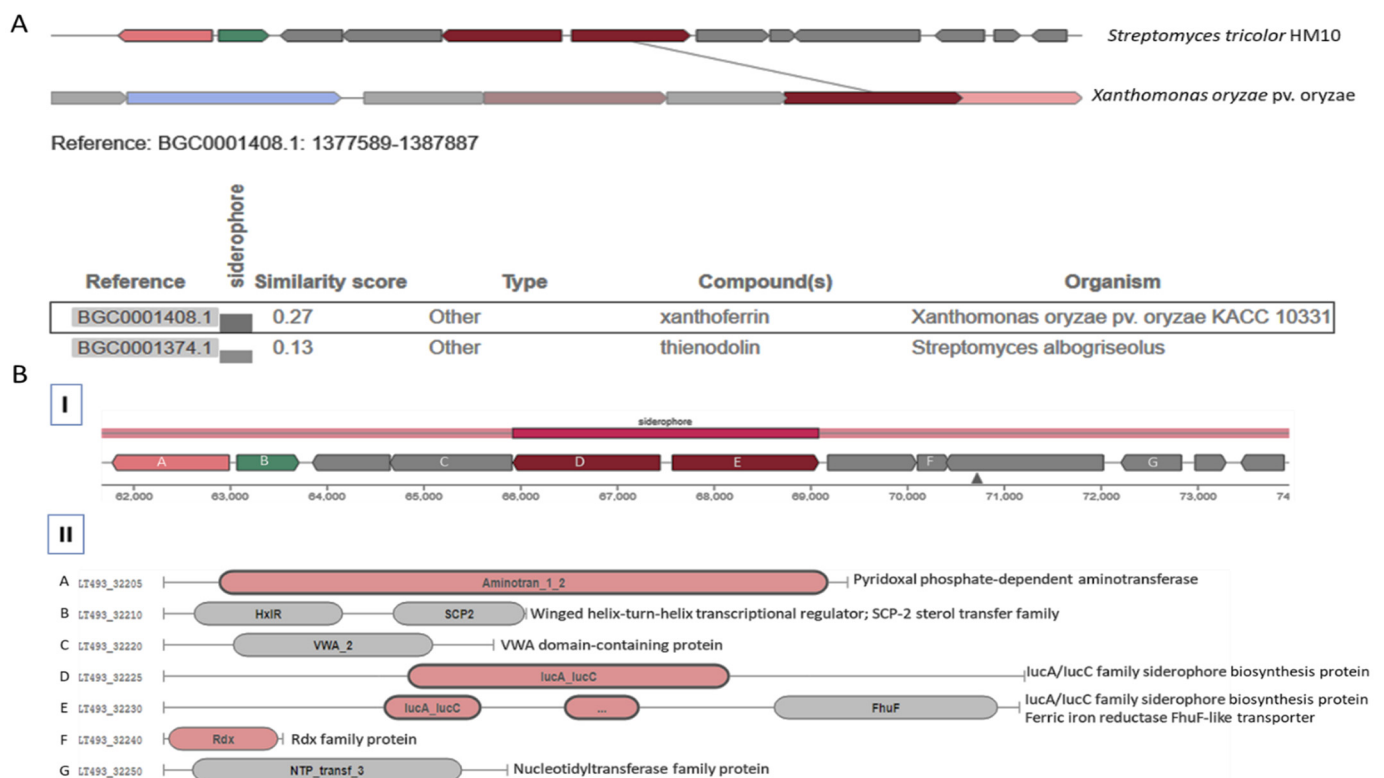


Figure 5. (A) The comparison between the proposed carboxylate-type siderophore gene cluster (dark red gene) in *S. tricolor* HM10 and the proposed identified xanthoferrin siderophore pathway in *Xanthomonas oryzae* with a similarity score of 0.27 on the MIBiG website. (B) The proposed carboxylate gene cluster in *S. tricolor* HM10 was determined based on the Pfam website. (I) Siderophore gene cluster in contig_52.1 from the genome sequence; (II) genes involved in siderophore biosynthesis: A, pyridoxal phosphate-dependent aminotransferase; B, transcriptional regulator; C, VWA domain-containing protein; D, IucA/IucC family siderophore biosynthesis protein; E, IucA/IucC family siderophore biosynthesis protein and ferric iron reductase FhuF-like transporter; F, Rdx family protein (LT493_32240); and G, nucleotidyltransferase family protein.

3.4. Phylogenetic Analysis

The phylogenetic tree (Figure 6) represents the relationship between IucA/IucC family protein from the proposed catechol pathway in *S. tricolor* HM10 and isochorismate synthase genes (the proposed *SidC* gene) in identified catechol pathways in other bacteria. The IucA/IucC family protein showed an identity of 74% and positivity of 76% when compared to iron transporter (Rhbc) from the type strains *S. tricolor* and *Streptomyces* sp. FBKL.4005 (WP_094373031). In the proposed hydroximate pathway, the IucA/IucC family protein is separated into one clade with related proteins from *Streptomyces* (Gram-positive). In contrast, the similar protein from Gram-negative bacteria (*Vibrio mimicus*, *Pantoea ananatis*, *Shigella boydii*, and *Escherichia coli* K-12) separated into a second clade (Figure 7).

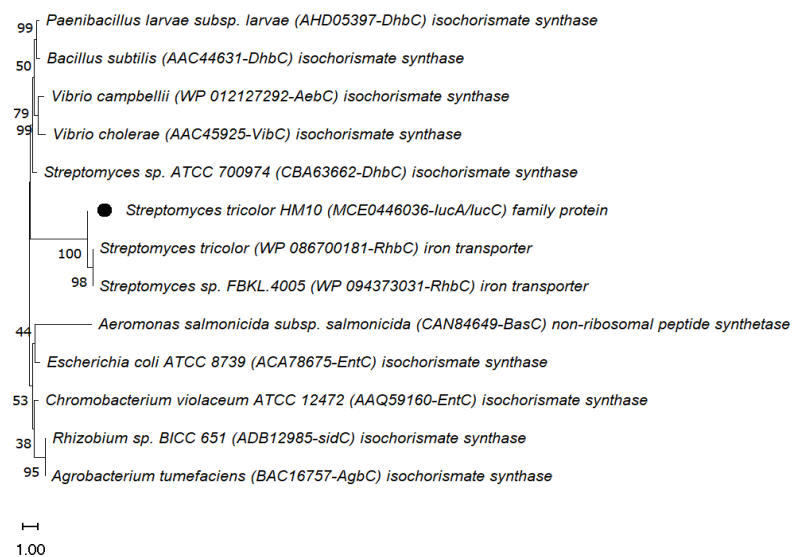


Figure 6. Constructed phylogenetic tree of the proposed IucA/IucC family protein in the *S. tricolor* HM10 catechol pathway with 12 protein sequences from other bacteria. The dendrogram was generated by the maximum likelihood, Jones–Taylor–Thornton (JTT) model, and nearest-neighbor-interchange (NNI) with 1000 bootstrap replicates (see the Methods section). The accession numbers of the SidC FASTA sequences are given.



Figure 7. Molecular phylogenetic analysis of IucA/IucC family protein in the hydroximate pathway compared with eight protein sequences from other bacteria. The dendrogram was generated by the maximum likelihood, Jones–Taylor–Thornton (JTT) model, and nearest-neighbor-interchange (NNI) with 1000 bootstrap replicates (see the Methods section). The accession numbers of the SidC FASTA sequences are given.

The IucA/IucC family protein from *S. tricolor* HM10 exhibited 91% and 92% identities and positives, respectively, with the IucA/IucC family siderophore biosynthesis protein from *S. dioscori* and *S. aurantiacus*. In the case of the carboxylate siderophore pathway, the IucA/IucC family protein from *S. tricolor* HM10 was closely related to a similar protein in *Streptomyces* sp. FBKL 4005 (Figure 8).

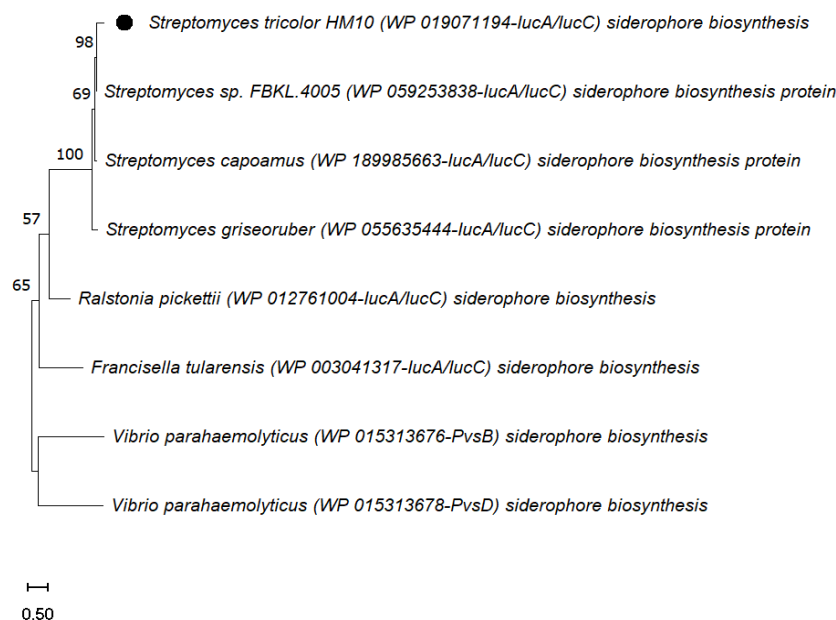


Figure 8. Molecular phylogenetic analysis of IucA/IucC family protein in the carboxylate pathway compared with seven protein sequences from other bacteria. The dendrogram was generated by the maximum likelihood, Jones–Taylor–Thornton (JTT) model, and nearest-neighbor-interchange (NNI) with 1000 bootstrap replicates (see the Methods section). The accession numbers of the SidC FASTA sequences are given.

4. Discussion

Siderophores are small and low-molecular-weight metabolites with high affinity to chelate the ferric iron. A variety of microorganisms such as *Streptomyces* widely produce these secondary metabolites. *Streptomyces* are numerous soil microbes, widely distributed, and an excellent source of secondary metabolites and bioactive compounds such as antibiotics, siderophores, and extracellular enzymes [55]. The *Streptomyces* genus can produce a wide variety of siderophore types, and a specific strain can produce more than one siderophore compound [35,38,56].

S. tricolor HM10 produces three different types of siderophores. It can produce a catechol-type siderophore with up to 6 µg/mL equivalent of 2,3-DHBA. Moreover, hydroxamate and carboxylate types are produced by the same strain. Ferreira et al. [57] reported that five strains (*Rhizobium radiobacter*, *Bacillus megaterium*, *Azotobacter vinelandii*, *Bacillus subtilis*, and *Pantoea allii*) could produce the maximum siderophore amount (80–140 µmol L⁻¹) after 24–48 h, except *A. vinelandii*, which produced the same amount after 72 h. The amount of hydroxamate siderophore produced was 18.18 mg/L in *Pseudomonas aeruginosa* FP6 [58], whereas Gull and Hafeez (2012) [59] reported 15.5 µg/mL of hydroxamate siderophore in *Pseudomonas fluorescens* Mst 8.2. *S. tricolor* HM10 produced the hydroxamate type with absorbance reaching 0.062 at 480 nm and 0.13 of the carboxylate type when the absorbance was measured in the 200–280-nm range. Using the CAS assay, Rondon et al. [60] measured siderophore production by *Agrobacterium tumefaciens* C58. The absorbance at OD₅₉₀ reached 0.6 in wild-type culture. Similar results were detected in catechol production by *Rhizobium leguminosarum* strain IARI 312 grown in a modified Fiss minimal medium (0.6 at OD₅₀₀) [61]. The standard curve by Sumei et al. [62] indicated that 0.43 at OD₅₂₀ reflected the presence of 6 µg/mL from hydroxamate-type siderophores. Furthermore,

Rhizobium strain 22 produced the hydroxamate siderophore in a Fiss-glucose medium (0.2 at OD₄₈₀) [63]. In the case of the catechol siderophore, *S. tricolor* strain HM10 produced a lower amount (6 µg/mL) compared to the previous mentioned organisms. When compared to other mentioned microbes, *S. tricolor* HM10 also exhibited a lower absorbance, reflecting less production of hydroxamate and carboxylate siderophores. Otherwise, strain HM10 was distinguished by the production of three different siderophore-types (catechol, hydroxamate, and carboxylate).

In *S. coelicolor* A3(2) and *S. ambofaciens* ATCC 23877, the three tris-hydroxamate iron-chelators desferrioxamine B, E, and coelichelin have been reported to be produced by des and cch clusters. Sequence analyses of both clusters suggested that ferric-siderophore uptake systems are also encoded by each cluster [64,65]. Furthermore, *S. viridosporus* produces two different siderophores: desferrioxamine B (the linear siderophore) and desferrioxamine E (the cyclic one), whereas the linear desferrioxamine G considers the major product form of *S. coelicolor* and *S. lividans* [36]. The familiar desferrioxamine siderophore is produced by both *S. chartreusis* and *S. atratus* SCSIOZH16.

The genome analysis of *S. tricolor* HM10 revealed three possible pathways related to siderophore production. The catechol pathway comprises five genes that encode acetyltransferase, iron transporter, IucA/IucC family protein, ferric iron reductase FhuF, and aminotransferase. N-acetyltransferase enzyme-implicated iron acquisition occurs in *Pseudomonas cichorii* strain SPC9018 [66]. In *Pseudomonas aeruginosa* PAO1, aminotransferase catalyzes the aminotransferase reaction by converting aspartate β-semialdehyde and l-2,4-diaminobutyrate during pyoverdine siderophore biosynthesis [67]. IucA and IucC are non-ribosomal peptide synthetase (NRPS)-independent or -dependent enzymes. These enzymes have ligase activity, which activates and assembles a broad range of amino, carboxy, and hydroxy acids, resulting in high structural macrocyclic products [22,28]. Furthermore, hydroxamate and carboxylate siderophores are assembled by NRPS-independent mechanisms. FhuF, a ferric siderophore reductase (FSR), is involved in iron release from the siderophore inside the cell as described in *E. coli*. Otherwise, siderophore-interacting proteins (SIPs) perform the same process [68].

The *asbABCDEF* gene cluster from *Bacillus anthracis* is located in a single operon and is responsible for the biosynthesis of catechol siderophore petrobactin, which involves iron acquisition and virulence in the murine model of anthrax. A combination of AsbCDEF condenses spermidine and 3,4-dihydroxybenzoic acid. AsbF (3-dehydroshikimate dehydratase) converts 3-dehydroshikimate into 3,4-dihydroxybenzoic acid (DHB). AsbE (petrobactin synthase) functions in condensing 3,4-dihydroxybenzoyl-AsbD with spermidine to yield 3,4-dihydroxybenzoyl-spermidine citrate for petrobactin assembly. Furthermore, AsbC (3,4-dihydroxybenzoic acid-AMP ligase) considers the main component in the biosynthesis of DHB-spermidine (DHB-SP), whereas AsbB (3,4-dihydroxybenzoyl-citryl-spermidine: spermidine ligase) catalyzes the condensation of the second molecule from 3,4-dihydroxybenzoyl spermidine with 3,4-dihydroxybenzoyl spermidinyl citrate to form the mature siderophore. AsbA (spermidine-citrate ligase) performs condensation of 3,4-dihydroxybenzoyl spermidine with citrate to form 3,4-dihydroxybenzoyl spermidinyl citrate [69–76]. When compared with catechol siderophore by *S. tricolor* HM10, the presented petrobactin pathway shows broad differences. Strain HM10 is predicted to have acetyltransferase and aminotransferase enzymes that are missing in the petrobactin pathway, thus supporting the idea of a new catechol siderophore molecule. Based on bioinformatic analysis, petrobactin is the most closely related siderophore to the catechol type, with a similarity score of 0.17 on the MIBiG website. This value means there is a high probability of new siderophore biosynthesis from strain HM10.

The proposed hydroxamate pathway in *S. tricolor* HM10 involves eight genes that encode a siderophore-interacting protein, lysine decarboxylase, lysine N(6)-hydroxylase/L-ornithine N(5)-oxygenase family protein, acetyltransferase, IucA/IucC family protein, ferric iron reductase FhuF-like transporter, beta-N-acetylhexosaminidase, and DUF4429 domain-containing protein. In *S. coelicolor* A3 (2), the hydroxamate siderophore desferriox-

amine B/E pathways consist of clusters containing four genes (*desA-desD*). The desired pathway can be summarized: DesA (pyridoxal-dependent decarboxylase), which decarboxylates L-lysine to produce cadaverine; DesB (monooxygenase) oxidizes cadaverine to yield *N*-hydroxycadaverine; DesC (acyl-CoA-dependent acyltransferase) adds an acetyl group (succinyl group in the case of desferrioxamine E) to *N*-hydroxycadaverine, resulting in the *N*-acetyl-*N*-hydroxycadaverine (*N*-hydroxy-*N*-succinylcadaverine in the case of desferrioxamine E); and DesD (desferrioxamine biosynthesis protein) catalyzes the final NTP-dependent reaction between two molecules of *N*-hydroxy-*N*-succinylcadaverine and *N*-acetyl-*N*-hydroxycadaverine to produce desferrioxamine B (converts three molecules of *N*-hydroxy-*N*-succinylcadaverine into desferrioxamine E). The same desferrioxamine pathway was identified in some *Streptomyces* strains, (i.e., *Streptomyces avermitilis* K139, *S. svioceus*, *S. atratus* SCSIOZH16, and *S. pristinaespiralis* HCCB10218) [10,77–80].

From a comparison between the desferrioxamine B/E pathway in *S. tricolor* HM10 and other bacteria, we conclude that the entire gene cluster exists in the HM10 genome except for the *desF* gene (siderophore-binding protein), which may be located in another position in the genome. Furthermore, two genes for ferric reductases (siderophore-interacting protein and ferric iron reductase FhuF-like transporter) present in the proposed pathway are in the HM10 genome.

The third pathway has seven coding genes that produce pyridoxal phosphate-dependent aminotransferase, transcriptional regulator, VWA domain-containing protein, IucA/IucC family siderophore biosynthesis protein, IucA/IucC family siderophore biosynthesis protein, ferric iron reductase FhuF-like transporter, Rdx family protein, and nucleotidyltransferase family protein. The carboxylate-type siderophores are formed in various organisms. *Rhizopus microspores* produce Rhizoferrin [81,82] while Xanthoferrin is synthesized in *Xanthomonas campestris* pv. *campestris* and *Xanthomonas oryzae* pv. *oryzae* [83,84]. Furthermore, Vibrioferrin has been extracted from *Vibrio parahaemolyticus* [85]. Based on in silico analysis, the similarity between the identified carboxylate siderophore pathway in strain HM10 and the xanthoferrin pathway in *Xanthomonas oryzae* reached a score of 0.27 on the MIBiG website. Furthermore, some genes in the identified pathway are absent when compared with the xanthoferrin pathway (i.e., diaminopimelate decarboxylase and 4-hydroxy-2-oxovalerate aldolase) whereas other genes are extra (i.e., pyridoxal phosphate-dependent aminotransferase). This low similarity reflects the possibility of a new carboxylate siderophore.

Siderophores have great importance in many fields. In microbial ecology, siderophores enhance the growth of microorganisms in natural and artificial media and alter the microbial community [19]. In agriculture, siderophores promote plant growth since microbial siderophores might be considered an efficient iron source for plants [86,87]. Siderophores play a significant role in the biological control mechanism against certain phytopathogens via tightly binding with iron and reducing iron that is bioavailable for the plant pathogens, thus killing them [18]. Furthermore, siderophores enhance the bioremediation of heavy metals by detoxifying samples with heavy metal contamination by binding with a wide range of toxic metals, such as Cr³⁺, Al³⁺, Cu²⁺, Eu³⁺, and Pb²⁺ [19,88]. Siderophores as medicine can be used in a trojan horse strategy to deliver antibiotics to antibiotic-resistant bacteria [89], as an antimalarial agent against *Plasmodium falciparum* [90], and in cancer therapy since desferrioxamines were used to significantly decrease the growth of aggressive tumors in patients with neuroblastoma or leukemia [91].

5. Conclusions

Siderophores are secondary metabolites produced by various microorganisms, plants, and animals. *Streptomyces* produce a wide range of secondary metabolites, such as siderophores. The newly isolated strain *S. tricolor* HM10 exhibited a diverse production of siderophore types. It produced three different siderophore types: catechol, hydroximate, and carboxylate types. The proposed pathways related to the three types were identified based on complete genome analysis with bioinformatics tools after sequencing. The new strain is con-

sidered a promising source for siderophore production with the probability of identifying a new siderophore structure.

Supplementary Materials: The following supporting information can be downloaded at: <https://www.mdpi.com/article/10.3390/fermentation8080346/s1>, Figure S1: Catechol-type siderophore pathway in *S. tricolor* HM10 and the related bacteria with up to 85% similarity with *Streptomyces* sp. BK340 when compared in ClusterBlast. Figure S2: Hydroxamate-type siderophore pathway in *S. tricolor* HM10 and the associated bacteria with up to 100% similarity with *S. griseus* compared with KnownClusterBlast. Figure S3: Carboxylate-type siderophore pathway in *S. tricolor* HM10 and the related bacteria with up to 81% similarity with *S. griseoruber* DSM 40281 PRJNA2 when compared at ClusterBlast. Table S1: The statistics of the *S. tricolor* HM10 sequenced genome.

Author Contributions: All authors contributed to the research design. M.R. and H.B., designed and conducted the experiments. M.R., H.B., K.A.Q., I.S.A. and A.S.A. constructed and edited the manuscript. All authors have read and agreed to the published version of the manuscript.

Funding: Fund to perform the current research was received from Qassim University, represented by the Deanship of Scientific Research, for the financial support for this research under the number (CAVM-2019-2-2-I-5457) during the academic year 1440 AH/2019 AD.

Institutional Review Board Statement: Not applicable.

Informed Consent Statement: Not applicable.

Data Availability Statement: Data is contained within the article.

Acknowledgments: The authors gratefully acknowledge Qassim University, represented by the Deanship of Scientific Research, on the financial support for this research under the number (CAVM-2019-2-2-I-5457) during the academic year 1440 AH / 2019 AD. The authors thank Abdellatif Gueddou, Dept. of Molecular, Cellular, and Biomedical Sciences, University of New Hampshire, Durham, NH 03824, USA, for genome sequencing, assembly, and annotation and Louis Tisa for English revision.

Conflicts of Interest: The authors declare no conflict of interest.

References

1. Datta, B.; Chakrabartty, P.K. Siderophore Biosynthesis Genes of *Rhizobium* sp. Isolated from *Cicer arietinum* L. *3 Biotech* **2014**, *4*, 391–401. [[CrossRef](#)]
2. Searle, L.J.; Méric, G.; Porcelli, I.; Sheppard, S.K.; Lucchini, S. Variation in Siderophore Biosynthetic Gene Distribution and Production across Environmental and Faecal Populations of *Escherichia coli*. *PLoS ONE* **2015**, *10*, e0117906. [[CrossRef](#)]
3. Neilands, J.B. Siderophores: Structure and Function of Microbial Iron Transport Compounds. *J. Biol. Chem.* **1995**, *270*, 26723–26726. [[CrossRef](#)]
4. Kodani, S.; Bicz, J.; Song, L.; Deeth, R.; Ohnishi-Kameyama, M.; Yoshida, M.; Ochi, K.; Challis, G. ChemInform Abstract: Structure and Biosynthesis of Scabichelin, a Novel Tris-Hydroxamate Siderophore Produced by the Plant Pathogen *Streptomyces scabies* 87.22. *Org. Biomol. Chem.* **2013**, *11*, 4686–4694. [[CrossRef](#)]
5. Crosa, J.H.; Walsh, C.T. Genetics and Assembly Line Enzymology of Siderophore Biosynthesis in Bacteria. *Microbiol. Mol. Biol. Rev.* **2002**, *66*, 223–249. [[CrossRef](#)]
6. Winkelmann, G. Microbial Siderophore-Mediated Transport. *Biochem. Soc. Trans.* **2002**, *30*, 691–696. [[CrossRef](#)]
7. O'Brien, I.G.; Gibson, F. The Structure of Enterochelin and Related 2,3-dihydroxy-N-benzoyne Conjugates from *Escherichia coli*. *Biochim. Biophys. Acta Gen. Subj.* **1970**, *215*, 393–402. [[CrossRef](#)]
8. Moynié, L.; Milenkovic, S.; Mislin, G.L.A.; Gasser, V.; Mallocci, G.; Baco, E.; McCaughan, R.P.; Page, M.G.P.; Schalk, I.J.; Ceccarelli, M.; et al. The Complex of Ferric-Enterobactin with its Transporter from *Pseudomonas aeruginosa* Suggests a Two-Site Model. *Nat. Commun.* **2019**, *10*, 3673. [[CrossRef](#)]
9. Yamanaka, K.; Oikawa, H.; Ogawa, H.-o.; Hosono, K.; Shinmachi, F.; Takano, H.; Sakuda, S.; Beppu, T.; Ueda, K. Desferrioxamine E produced by *Streptomyces griseus* stimulates growth and development of *Streptomyces tanashiensis*. *Microbiology* **2005**, *151*, 2899–2905. [[CrossRef](#)]
10. Tunca, S.; Barreiro, C.; Sola-Landa, A.; Coque, J.J.R.; Martín, J.F. Transcriptional regulation of the desferrioxamine gene cluster of *Streptomyces coelicolor* is mediated by binding of DmdR1 to an iron box in the promoter of the desA gene. *FEBS J.* **2007**, *274*, 1110–1122. [[CrossRef](#)]
11. Cheung, J.; Beasley, F.C.; Liu, S.; Lajoie, G.A.; Heinrichs, D.E. Molecular Characterization of Staphyloferrin B Biosynthesis in *Staphylococcus aureus*. *Mol. Microbiol.* **2009**, *74*, 594–608. [[CrossRef](#)]

12. Hagan, A.K.; Plotnick, Y.M.; Dingle, R.E.; Mendel, Z.I.; Cendrowski, S.R.; Sherman, D.H.; Tripathi, A.; Hanna, P.C. Petrobactin Protects against Oxidative Stress and Enhances Sporulation Efficiency in *Bacillus anthracis* Sterne. *MBio* **2018**, *9*, e02079-18. [[CrossRef](#)]
13. Najimi, M.; Lemos, M.L.; Osorio, C.R. Identification of Siderophore Biosynthesis Genes Essential for Growth of *Aeromonas salmonicida* under Iron Limitation Conditions. *Appl. Environ. Microbiol.* **2008**, *74*, 2341–2348. [[CrossRef](#)]
14. Silva, M.G.; de Curcio, J.S.; Silva-Bailão, M.G.; Lima, R.M.; Tomazett, M.V.; de Souza, A.F.; Cruz-Leite, V.R.M.; Sbaraini, N.; Bailão, A.M.; Rodrigues, F.; et al. Molecular Characterization of Siderophore Biosynthesis in *Paracoccidioides brasiliensis*. *IMA Fungus* **2020**, *11*, 11. [[CrossRef](#)]
15. Gärdes, A.; Triana, C.; Amin, S.A.; Green, D.H.; Romano, A.; Trimble, L.; Carrano, C.J. Detection of Photoactive Siderophore Biosynthetic Genes in the Marine Environment. *BioMetals* **2013**, *26*, 507–516. [[CrossRef](#)]
16. Storey, E.P.; Boghoozian, R.; Little, J.L.; Lowman, D.W.; Chakraborty, R. Characterization of ‘Schizokinen’; A Dihydroxamate-type Siderophore Produced by *Rhizobium leguminosarum* IARI 917. *BioMetals* **2006**, *19*, 637–649. [[CrossRef](#)]
17. Raymond, K.N.; Dertz, E.A.; Kim, S.S. Enterobactin: An archetype for microbial iron transport. *Proc. Natl. Acad. Sci. USA* **2003**, *100*, 3584–3588. [[CrossRef](#)]
18. Ahmed, E.; Holmström, S.J.M. Siderophores in Environmental Research: Roles and Applications. *Microb. Biotechnol.* **2014**, *7*, 196–208. [[CrossRef](#)]
19. Saha, M.; Sarkar, S.; Sarkar, B.; Sharma, B.K.; Bhattacharjee, S.; Tribedi, P. Microbial Siderophores and their Potential Applications: A Review. *Environ. Sci. Pollut. Res.* **2016**, *23*, 3984–3999. [[CrossRef](#)]
20. Górska, A.; Sloderbach, A.; Marszałł, M.P. Siderophore-Drug Complexes: Potential Medicinal Applications of the ‘Trojan horse’ Strategy. *Trends Pharmacol. Sci.* **2014**, *35*, 442–449. [[CrossRef](#)]
21. De Serrano, L.O. Biotechnology of Siderophores in High-Impact Scientific Fields. *Biomol. Concepts* **2017**, *8*, 169–178. [[CrossRef](#)]
22. Kurth, C.; Kage, H.; Nett, M. Siderophores as Molecular Tools in Medical and Environmental Applications. *Org. Biomol. Chem.* **2016**, *14*, 8212–8227. [[CrossRef](#)]
23. Fan, D.; Fang, Q. Siderophores for Medical Applications: Imaging, Sensors, and Therapeutics. *Int. J. Pharm.* **2021**, *597*, 120306. [[CrossRef](#)]
24. Albelda-Berenguer, M.; Monachon, M.; Joseph, E. *Chapter Five—Siderophores: From Natural Roles to Potential Applications*; Gadd, G.M., Sariaslani, S.B.T.A.i.A.M., Eds.; Academic Press: Cambridge, MA, USA, 2019; Volume 106, pp. 193–225.
25. Dimkpa, C. Microbial Siderophores: Production, Detection and Application in Agriculture and Environment. *Endocytobiosis Cell Res.* **2016**, *27*, 7–16.
26. Rapti, S.; Boyatzis, S.C.; Rivers, S.; Pournou, A. *Siderophores and their Applications in Wood, Textile, and Paper Conservation BT—Microorganisms in the Deterioration and Preservation of Cultural Heritage*; Joseph, E., Ed.; Springer International Publishing: Cham, Switzerland, 2021; pp. 301–339.
27. Hofmann, M.; Heine, T.; Malik, L.; Hofmann, S.; Joffroy, K.; Senges, C.H.; Bandow, J.E.; Tischler, D. Screening for Microbial Metal-Chelating Siderophores for the Removal of Metal Ions from Solutions. *Microorganisms* **2021**, *9*, 111. [[CrossRef](#)]
28. Miethke, M.; Marahiel, M.A. Siderophore-Based Iron Acquisition and Pathogen Control. *Microbiol. Mol. Biol. Rev.* **2007**, *71*, 413–451. [[CrossRef](#)]
29. Bannerman, R.M.; Callender, S.T.; Williams, D.L. Effect of Desferrioxamine and D.T.P.A. in Iron Overload. *Br. Med. J.* **1962**, *2*, 1573–1577. [[CrossRef](#)]
30. Khan, A.; Singh, P.; Srivastava, A. Synthesis, Nature and Utility of Universal Iron Chelator—Siderophore: A review. *Microbiol. Res.* **2018**, *212*, 103–111. [[CrossRef](#)]
31. Boyce, J.H.; Dang, B.; Ary, B.; Edmondson, Q.; Craik, C.S.; DeGrado, W.F.; Seiple, I.B. Platform to Discover Protease-Activated Antibiotics and Application to Siderophore–Antibiotic Conjugates. *J. Am. Chem. Soc.* **2020**, *142*, 21310–21321. [[CrossRef](#)]
32. Saha, P.; Yeoh, B.S.; Xiao, X.; Golonka, R.M.; Kumarasamy, S.; Vijay-Kumar, M. Enterobactin, an iron chelating bacterial siderophore, arrests cancer cell proliferation. *Biochem. Pharmacol.* **2019**, *168*, 71–81. [[CrossRef](#)]
33. Ribeiro, M.; Simões, M. Advances in the Antimicrobial and Therapeutic Potential of Siderophores. *Environ. Chem. Lett.* **2019**, *17*, 1485–1494. [[CrossRef](#)]
34. Zumla, A.; Rao, M.; Wallis, R.S.; Kaufmann, S.H.E.; Rustomjee, R.; Mwaba, P.; Vilaplana, C.; Yeboah-Manu, D.; Chakaya, J.; Ippolito, G.; et al. Host-Directed Therapies for Infectious Diseases: Current Status, Recent Progress, and Future Prospects. *Lancet Infect. Dis.* **2016**, *16*, e47–e63. [[CrossRef](#)]
35. Dimkpa, C.; Svatoš, A.; Merten, D.; Büchel, G.; Kothe, E. Hydroxamate Siderophores Produced by *Streptomyces acidiscabies* E13 Bind Nickel and Promote Growth in Cowpea (*Vigna unguiculata* L.) under Nickel Stress. *Can. J. Microbiol.* **2008**, *54*, 163–172. [[CrossRef](#)] [[PubMed](#)]
36. Imbert, M.; Béchet, M.; Blondeau, R. Comparison of the Main Siderophores Produced by some Species of *Streptomyces*. *Curr. Microbiol.* **1995**, *31*, 129–133. [[CrossRef](#)]
37. Patel, P.; Song, L.; Challis, G.L. Distinct Extracytoplasmic Siderophore Binding Proteins Recognize Ferrioxamines and Ferri-coelichelin in *Streptomyces coelicolor* A3(2). *Biochemistry* **2010**, *49*, 8033–8042. [[CrossRef](#)]
38. Armin, R.; Zühlke, S.; Grunewaldt-Stöcker, G.; Mahnkopp-Dirks, F.; Kusari, S. Production of Siderophores by an Apple Root-Associated *Streptomyces ciscaucasicus* Strain GS2 Using Chemical and Biological OSMAC Approaches. *Molecules* **2021**, *26*, 562. [[CrossRef](#)]

39. Chen, J.; Guo, Y.; Lu, Y.; Wang, B.; Sun, J.; Zhang, H.; Wang, H. Chemistry and Biology of Siderophores from Marine Microbes. *Mar. Drugs* **2019**, *17*, 562. [CrossRef]
40. Matsuo, Y.; Kanoh, K.; Jang, J.-H.; Adachi, K.; Matsuda, S.; Miki, O.; Kato, T.; Shizuri, Y. Streptobactin, a Triccatechol-Type Siderophore from Marine-Derived *Streptomyces* sp. YM5-799. *J. Nat. Prod.* **2011**, *74*, 2371–2376. [CrossRef]
41. Rai, V.; Fisher, N.; Duckworth, O.W.; Baars, O. Extraction and Detection of Structurally Diverse Siderophores in Soil. *Front. Microbiol.* **2020**, *11*, 2165. [CrossRef]
42. Rehan, M.; Alshim, A.S.; Abidou, H.; Rasheed, Z.; Al Abdulmonem, W. Isolation, Identification, Biocontrol Activity, and Plant Growth Promoting Capability of a Superior *Streptomyces tricolor* Strain HM10. *Pol. J. Microbiol.* **2021**, *70*, 245–256. [CrossRef]
43. Schwyn, B.; Neilands, J.B. Universal Chemical Assay for the Detection and Determination of Siderophores. *Anal. Biochem.* **1987**, *160*, 47–56. [CrossRef]
44. Arnow, L.E. Colorimetric Determination of the Components of 3,4-dihydroxyphenylalaninetyrosine Mixtures. *J. Biol. Chem.* **1937**, *118*, 531–537. [CrossRef]
45. Atkin, C.L.; Neilands, J.B.; Phaff, H.J. Rhodotorulic Acid from Species of *Leucosporidium*, *Rhodospiridium*, *Rhodotorula*, *Sporidiobolus*, and *Sporobolomyces*, and A New Alanine-Containing Ferrichrome from *Cryptococcus melibiosum*. *J. Bacteriol.* **1970**, *103*, 722–733. [CrossRef] [PubMed]
46. Shenker, M.; Chen, Y.; Ghirlando, R.; Oliver, I.; Helmann, M.; Hadar, Y. Chemical Structure and Biological Activity of A Siderophore Produced by *Rhizopus arrhizus*. *Soil Sci. Soc. Am. J.* **1995**, *59*, 837–843. [CrossRef]
47. Aboul-Maaty, N.A.-F.; Oraby, H.A.-S. Extraction of High-Quality Genomic DNA from different Plant Orders Applying A Modified CTAB-Based Method. *Bull. Natl. Res. Cent.* **2019**, *43*, 25. [CrossRef]
48. Kolmogorov, M.; Yuan, J.; Lin, Y.; Pevzner, P.A. Assembly of Long, Error-prone Reads Using Repeat Graphs. *Nat. Biotechnol.* **2019**, *37*, 540–546. [CrossRef]
49. Meier-Kolthoff, J.P.; Göker, M. TYGS is an Automated High-Throughput Platform for State-of-the-Art Genome-Based Taxonomy. *Nat. Commun.* **2019**, *10*, 2182. [CrossRef]
50. Blin, K.; Shaw, S.; Kloosterman, A.M.; Charlop-Powers, Z.; van Wezel, G.P.; Medema, M.H.; Weber, T. AntiSMASH 6.0: Improving Cluster Detection and Comparison Capabilities. *Nucleic Acids Res.* **2021**, *49*, W29–W35. [CrossRef]
51. Mistry, J.; Chuguransky, S.; Williams, L.; Qureshi, M.; Salazar, G.A.; Sonnhammer, E.L.L.; Tosatto, S.C.E.; Paladin, L.; Raj, S.; Richardson, L.J.; et al. Pfam: The Protein Families Database in 2021. *Nucleic Acids Res.* **2021**, *49*, D412–D419. [CrossRef]
52. Kautsar, S.A.; Blin, K.; Shaw, S.; Navarro-Muñoz, J.C.; Terlouw, B.R.; van der Hooft, J.J.J.; van Santen, J.A.; Tracanna, V.; Suarez Duran, H.G.; Pascal Andreu, V.; et al. MIBiG 2.0: A repository for biosynthetic gene clusters of known function. *Nucleic Acids Res.* **2020**, *48*, D454–D458. [CrossRef]
53. Tamura, K.; Stecher, G.; Kumar, S. MEGA11: Molecular Evolutionary Genetics Analysis Version 11. *Mol. Biol. Evol.* **2021**, *38*, 3022–3027. [CrossRef] [PubMed]
54. France, S. STATISTICA (Logiciel D’analyse de Données), Version 7.1. 2005. Available online: www.statsoft.fr (accessed on 16 June 2022).
55. Olanrewaju, O.S.; Babalola, O.O. Streptomyces: Implications and Interactions in Plant Growth Promotion. *Appl. Microbiol. Biotechnol.* **2019**, *103*, 1179–1188. [CrossRef] [PubMed]
56. van Bergeijk, D.A.; Elsayed, S.S.; Du, C.; Santiago, I.N.; Roseboom, A.M.; Zhang, L.; Carrión, V.J.; Spaink, H.P.; van Wezel, G.P. The Ubiquitous Catechol Moiety Elicits Siderophore and Angucycline Production in *Streptomyces*. *Commun. Chem.* **2022**, *5*, 14. [CrossRef]
57. Ferreira, C.M.H.; Vilas-Boas, Â.; Sousa, C.A.; Soares, H.M.V.M.; Soares, E.V. Comparison of Five Bacterial Strains Producing Siderophores with Ability to Chelate Iron Under Alkaline Conditions. *AMB Express* **2019**, *9*, 78. [CrossRef]
58. Sasirekha, B.; Srividya, S. Siderophore Production by *Pseudomonas aeruginosa* FP6, a Biocontrol Strain for *Rhizoctonia solani* and *Colletotrichum gloeosporioides* Causing Diseases in Chilli. *Agric. Nat. Resour.* **2016**, *50*, 250–256. [CrossRef]
59. Gull, M.; Hafeez, F.Y. Characterization of siderophore producing bacterial strain *Pseudomonas fluorescens* Mst 8.2 as plant growth promoting and biocontrol agent in wheat. *Afr. J. Microbiol. Res.* **2012**, *6*, 6308–6318. [CrossRef]
60. Rondon, M.R.; Ballering, K.S.; Thomas, M.G. Identification and Analysis of A Siderophore Biosynthetic Gene Cluster from *Agrobacterium tumefaciens* C58. *Microbiology* **2004**, *150*, 3857–3866. [CrossRef]
61. Clark, B.L. *Characterization of A Catechol-Type Siderophore and the Detection of A Possible Outer Membrane Receptor Protein from Rhizobium leguminosarum Strain IARI 312*; East Tennessee State University: Ann Arbor, MI, USA, 2004.
62. Sumei, Y.; Chunying, T.; Xin, B.; Jinsong, L.; Tao, S.; Liying, D.; Yu, J. Optimization of Siderophore Production by *Bacillus* sp. PZ-1 and Its Potential Enhancement of Phytoextraction of Pb from Soi. *J. Microbiol. Biotechnol.* **2017**, *27*, 1500–1512. [CrossRef]
63. Sridevi, M.; Mallaiiah, K. Production of Catechol-Type of Siderophores by *Rhizobium* Strains from *Sesbania sesban* (L.) Merr. *Asian J. Bio Sci.* **2008**, *3*, 187–194.
64. Barona-Gómez, F.; Lautru, S.; Francou, F.-X.; Leblond, P.; Pernodet, J.-L.; Challis, G. Multiple Biosynthetic and Uptake Systems Mediate Siderophore-Dependent Iron Acquisition in *Streptomyces coelicolor* A3(2) and *Streptomyces ambifaciens* ATCC 23877. *Microbiology* **2006**, *152*, 3355–3366. [CrossRef] [PubMed]

65. Patel, P. *Investigations of Streptomyces coelicolor A3 (2) Siderophore Sinding Proteins*; University of Warwick: Coventry, UK, 2009.
66. Wali, U.M.; Mori, Y.; Maenaka, R.; Kai, K.; Tanaka, M.; Ohnishi, K.; Kiba, A.; Hikichi, Y. The N-acetyltransferase Gene-implicated Iron Acquisition Contributes to Host Specificity of *Pseudomonas cichorii* Strain SPC9018 and its Virulence. *Physiol. Mol. Plant Pathol.* **2015**, *92*, 14–21. [[CrossRef](#)]
67. Vandenende, C.S.; Vlasschaert, M.; Seah, S.Y.K. Functional Characterization of an Aminotransferase Required for Pyoverdine Siderophore Biosynthesis in *Pseudomonas aeruginosa* PAO1. *J. Bacteriol.* **2004**, *186*, 5596–5602. [[CrossRef](#)]
68. Trindade, I.B.; Hernandez, G.; Lebègue, E.; Barrière, F.; Cordeiro, T.; Piccioli, M.; Louro, R.O. Conjuring up A Ghost: Structural and Functional Characterization of FhuF, A Ferric Siderophore Reductase from *E. coli*. *J. Biol. Inorg. Chem.* **2021**, *26*, 313–326. [[CrossRef](#)]
69. Fox, D.T.; Hotta, K.; Kim, C.-Y.; Koppisch, A.T. The Missing Link in Petrobactin Biosynthesis: AsbF Encodes a (–)-3-Dehydroshikimate Dehydratase. *Biochemistry* **2008**, *47*, 12251–12253. [[CrossRef](#)]
70. Hagan, A.; Tripathi, A.; Berger, D.; Sherman, D.; Hanna, P. Petrobactin Is Exported from *Bacillus anthracis* by the RND-Type Exporter ApeX. *mBio* **2017**, *8*, e01238-17. [[CrossRef](#)] [[PubMed](#)]
71. Koppisch, A.T.; Browder, C.C.; Moe, A.L.; Shelley, J.T.; Kinkel, B.A.; Hersman, L.E.; Iyer, S.; Ruggiero, C.E. Petrobactin is the Primary Siderophore Synthesized by *Bacillus anthracis* Str. Sterne under Conditions of Iron Starvation. *Biometals* **2005**, *18*, 577–585. [[CrossRef](#)]
72. Lee, J.Y.; Janes, B.K.; Passalacqua, K.D.; Pflieger, B.F.; Bergman, N.H.; Liu, H.; Håkansson, K.; Somu, R.V.; Aldrich, C.C.; Cendrowski, S.; et al. Biosynthetic Analysis of the Petrobactin Siderophore Pathway from *Bacillus anthracis*. *J. Bacteriol.* **2007**, *189*, 1698–1710. [[CrossRef](#)]
73. Lee, J.Y.; Passalacqua, K.D.; Hanna, P.C.; Sherman, D.H. Regulation of Petrobactin and Bacillibactin Biosynthesis in *Bacillus anthracis* under Iron and Oxygen Variation. *PLoS ONE* **2011**, *6*, e20777. [[CrossRef](#)] [[PubMed](#)]
74. Nusca, T.; Kim, Y.; Maltseva, N.; Lee, J.; Eschenfeldt, W.; Stols, L.; Schofield, M.; Scaglione, J.; Dixon, S.; Oves-Costales, D.; et al. Functional and Structural Analysis of the Siderophore Synthetase AsbB through Reconstitution of the Petrobactin Biosynthetic Pathway from *Bacillus anthracis*. *J. Biol. Chem.* **2012**, *287*, 16058–16072. [[CrossRef](#)] [[PubMed](#)]
75. Pflieger, B.F.; Kim, Y.; Nusca, T.D.; Maltseva, N.; Lee, J.Y.; Rath, C.M.; Scaglione, J.B.; Janes, B.K.; Anderson, E.C.; Bergman, N.H.; et al. Structural and Functional Analysis of AsbF: Origin of the Stealth 3,4-dihydroxybenzoic Acid Subunit for Petrobactin Biosynthesis. *Proc. Natl. Acad. Sci. USA* **2008**, *105*, 17133–17138. [[CrossRef](#)]
76. Pflieger, B.F.; Lee, J.Y.; Somu, R.V.; Aldrich, C.C.; Hanna, P.C.; Sherman, D.H. Characterization and Analysis of Early Enzymes for Petrobactin Biosynthesis in *Bacillus anthracis*. *Biochemistry* **2007**, *46*, 4147–4157. [[CrossRef](#)] [[PubMed](#)]
77. Barona-Gómez, F.; Wong, U.; Giannakopoulos, A.E.; Derrick, P.J.; Challis, G.L. Identification of a Cluster of Genes that Directs Desferrioxamine Biosynthesis in *Streptomyces coelicolor* M145. *J. Am. Chem. Soc.* **2004**, *126*, 16282–16283. [[CrossRef](#)] [[PubMed](#)]
78. Challis, G.L. Exploitation of the *Streptomyces coelicolor* A3(2) Genome Sequence for Discovery of New Natural Products and Biosynthetic Pathways. *J. Ind. Microbiol. Biotechnol.* **2014**, *41*, 219–232. [[CrossRef](#)] [[PubMed](#)]
79. Günter, K.; Toupet, C.; Schupp, T. Characterization of an Iron-Regulated Promoter involved in Desferrioxamine B Synthesis in *Streptomyces pilosus*: Repressor-Binding Site and Homology to the Diphtheria Toxin Gene Promoter. *J. Bacteriol.* **1993**, *175*, 3295–3302. [[CrossRef](#)]
80. Ronan, J.L.; Kadi, N.; McMahon, S.A.; Naismith, J.H.; Alkhalaf, L.M.; Challis, G.L. Desferrioxamine Biosynthesis: Diverse Hydroxamate Assembly by Substrate-Tolerant Acyl Transferase DesC. *Philos. Trans. R. Soc. Lond. B Biol. Sci.* **2018**, *373*, 20170068. [[CrossRef](#)]
81. Drechsel, H.; Tschierske, M.; Thieken, A.; Jung, G.; Zähler, H.; Winkelmann, G. The Carboxylate Type Siderophore Rhizoferrin and its Analogs Produced by Directed Fermentation. *J. Ind. Microbiol.* **1995**, *14*, 105–112. [[CrossRef](#)]
82. Li, B.; Deng, X.; Kim, S.H.; Buhrow, L.; Tomchick, D.R.; Phillips, M.A.; Michael, A.J. Alternative Pathways Utilize or Circumvent Putrescine for Biosynthesis of Putrescine-Containing Rhizoferrin. *J. Biol. Chem.* **2021**, *296*, 100146. [[CrossRef](#)]
83. Pandey, A.; Sonti, R.V. Role of the FeoB Protein and Siderophore in Promoting Virulence of *Xanthomonas oryzae* pv. *oryzae* on Rice. *J. Bacteriol.* **2010**, *192*, 3187–3203. [[CrossRef](#)]
84. Pandey, S.S.; Patnana, P.K.; Rai, R.; Chatterjee, S. Xanthoferrin, the α -hydroxycarboxylate-Type Siderophore of *Xanthomonas campestris* pv. *campestris*, is Required for Optimum Virulence and Growth Inside Cabbage. *Mol. Plant Pathol.* **2017**, *18*, 949–962. [[CrossRef](#)]
85. Thode, S.K.; Rojek, E.; Kozłowski, M.; Ahmad, R.; Haugen, P. Distribution of Siderophore Gene Systems on a Vibrionaceae phylogeny: Database Searches, Phylogenetic Analyses and Evolutionary Perspectives. *PLoS ONE* **2018**, *13*, e0191860. [[CrossRef](#)]
86. Crowley, D.E. *Microbial Siderophores in the Plant Rhizosphere BT—Iron Nutrition in Plants and Rhizospheric Microorganisms*; Barton, L.L., Abadia, J., Eds.; Springer: Dordrecht, The Netherlands, 2006; pp. 169–198.
87. Masalha, J.; Kosegarten, H.; Elmaci, Ö.; Mengel, K. The Central Role of Microbial Activity for Iron Acquisition in Maize and Sunflower. *Biol. Fertil. Soils* **2000**, *30*, 433–439. [[CrossRef](#)]
88. O'Brien, S.; Hodgson, D.J.; Buckling, A. Social Evolution of Toxic Metal Bioremediation in *Pseudomonas aeruginosa*. *Proc. R. Soc. B Biol. Sci.* **2014**, *281*, 20140858. [[CrossRef](#)] [[PubMed](#)]
89. Ye, J.; Liu, E.; Yu, Z.; Pei, X.; Chen, S.; Zhang, P.; Shin, M.-C.; Gong, J.; He, H.; Yang, V.C. CPP-Assisted Intracellular Drug Delivery, What Is Next? *Int. J. Mol. Sci.* **2016**, *17*, 1892. [[CrossRef](#)] [[PubMed](#)]

-
90. Tsafack, A.; Libman, J.; Shanzer, A.; Cabantchik, Z.I. Chemical Determinants of Antimalarial Activity of Reversed Siderophores. *Antimicrob. Agents Chemother.* **1996**, *40*, 2160–2166. [[CrossRef](#)]
 91. Lovejoy, B.D.; Richardson, R.D. Iron Chelators as Anti-Neoplastic Agents: Current Developments and Promise of the PIH Class of Chelators. *Curr. Med. Chem.* **2003**, *10*, 1035–1049. [[CrossRef](#)]